

Chlorinated diketopyrrolopyrrole dye exhibits a three-step polymorphic transition with thermosalient effects

Yusuke Kikuchi, Shinya Matsumoto*

Graduate School of Environment and Information Sciences, Yokohama National University, 79-7 Tokiwadai, Hodogaya-ku, Yokohama 240-8501, Japan.

Abstract

A tetramorphic system was discovered in a diketopyrrolopyrrole dye (3,6-bis(4-chlorophenyl)-2-propyl-2,5-dihydropyrrolo[3,4-c]pyrrole-1,4-dione), with thermosalient effects during thermal phase transitions. Two polymorphs, the red and orange forms, were obtained using liquid-liquid and liquid-gas diffusion. The other two polymorphs, the vermilion and deep red forms, were obtained by a thermal phase transition from the red and orange forms, respectively. The orange form was also prepared by a thermal phase transition from the vermilion form. Crystallinity was maintained during these thermal phase transitions. The thermosalient effect was also observed during each phase transition, with crystal deformation as the major observed effect. The molecular and crystal structures of the red, orange, and vermilion forms were analysed in terms of structural similarity and the intermolecular interactions.

Keywords

Thermosalient effect, Diketopyrrolopyrrole (DPP), Tetramorphic system, Phase transition

*Corresponding author. Tel +81-45-339-3366; Fax +81-45-339-3345. *E-mail address*: matsumoto-shinya-py@ynu.ac.jp (Shinya Matsumoto)

Introduction

There have been numerous studies on the responses of organic crystals to external stimuli in recent years [1], including organic crystals that reversibly change shape and size in response to external stimuli, such as heat and light, that have been applied in actuators [2], artificial muscles [3], and biomimetic devices [4]. The dynamic behaviour of organic crystals under thermal stimuli was initially reported by Etter et al. in 1993 [5], whereafter this phenomenon was denoted as the thermosalient effect. This is generally characterised by a phase transition with anisotropic lattice changes and structural similarities before and after the transition, although the reported variations of this effect and the related phenomena are diverse.

One of the organic dye reported to exhibit a thermosalient effect is a diketopyrrolopyrrole (DPP) derivative. DPP is commercially significant because of its good fastness and bright red colour in the solid state [6]. It has also been studied as a functional dye for optoelectronic materials, such as organic, light-emitting diodes [7], semiconductors [8], and solar cells [9]. Few studies have reported on its thermal phase transition behaviour, and in 2018, So et. al. discovered that crystals of chlorinated DPP with a propyl substituent on both amino groups (**PR3**) exhibited thermosalient effects, such as jumps and explosions [10, 11]. This dynamic motion was confirmed by the irreversible phase transition between the two polymorphs, and the flexible propyl groups and Cl atoms were critical to the observed transition.

We attempted monopropyl-substituted chlorinated DPP (**PRM3**, shown in Figure 1) synthesis to investigate its polymorphic behaviour and thermosalient effect. We discovered two different-coloured polymorphs of **PRM3** from crystallisation at 298 K: a red polymorph (**PRM3R**) and an orange polymorph (**PRM3O**). During an examination of the effects of heating on both polymorphs, we discovered a third different-coloured polymorph from **PRM3R**. The third, dark-vermilion polymorph, denoted **PRM3V**, underwent a phase change to **PRM3O** upon heating, accompanied by irreversible dynamic motion within the crystals. **PRM3O** then transformed to a fourth, dark-red polymorph (**PRM3DR**) upon careful heating, and dynamic motion was also observed in this transformation. **PRM3DR** was found to be stable under ambient conditions. An organic crystal rarely exhibits a stepwise phase transition while maintaining its crystallinity [12]. This study reports the crystal structures of three successfully analysed polymorphs of **PRM3** with observed thermosalient effects, revealing a remarkable organic crystal with thermal motion.

<Fig. 1>

Experimental

1. Materials and equipment

All materials in this study were of high purity and were used without further purification. 3,6-Bis(4-chlorophenyl)-2,5-dihydropyrrolo[3,4-c]pyrrole-1,4-dione (Pigment Red 254) was obtained from DIC Co. *t*-BuOK and 1-iodopropane were obtained from Tokyo Chemical Industry Co., Ltd. Dimethyl formamide (DMF) was purchased from Hayashi Pure Chemical Ind., Ltd. Wako silica gel C-300 (45–

75 μm) was used for column chromatography. All solvents were obtained from Kanto Chemical Co. ^1H and ^{13}C nuclear magnetic resonance (NMR) spectra were recorded on a Jeol ECA-500 MHz NMR instrument (Jeol Co.) with tetramethylsilane as the internal standard. High resolution mass spectra (HRMS) were collected using a [LC] LaChromUltra/[MS] NanoFrontierLD spectrometer (Hitachi High-Technologies Co.). Infrared (IR) spectra were recorded using an FT/IR-6200 spectrophotometer (JASCO).

2. Synthesis of PRM3 [13]

A suspension of Pigment Red 254 (0.71 g, 2.0 mmol) and *t*-BuOK (0.67 g, 6.0 mmol) in dehydrated DMF (30 mL) was stirred at room temperature for 1 h in a N_2 atmosphere. A solution of 1-iodopropane (0.28 mL, 2.0 mmol) in DMF (3 mL) was then added dropwise, and the mixture was stirred at room temperature for 24 h. Distilled H_2O (400 mL) was then added, and the mixture was stirred for 1 h. Dichloromethane (DCM, 50 mL) was added, and the DCM layer was separated from the aqueous layer and then washed with H_2O several times using a separating funnel. After DCM evaporation, silica gel column chromatography was performed (ethyl acetate:DCM = 1:6), yielding the pure product as an orange solid (208 mg, yield 26 %).

m.p.: 268–270 $^\circ\text{C}$. IR (KBr pellet): ν 3145.33, 3081.89, 3051.8, 2973.7, 2950.55, 2973.42, 1650.77, 1614.13, 1590.02, 1494.56, 1442.49, 1413.57, 1149.37, 1094.4, 1012.45, 833.10, 712.57 cm^{-1} . ^1H NMR (500 MHz, CDCl_3), δ (ppm): 9.24 (*s*, 1H), 8.27–8.22 (*m*, 2H), 7.80–7.74 (*m*, 2H), 7.57–7.51 (*m*, 2H), 7.49–7.43 (*m*, 2H), 3.84–3.73 (*m*, 2H), 1.65 (*h*, $J = 7.5$ Hz, 2H), 0.88 (*t*, $J = 7.4$ Hz, 3H). ^{13}C NMR (100 MHz, CDCl_3), δ (ppm): 11.29, 22.96, 43.84, 110.08, 111.04, 125.97, 126.45, 129.17, 129.47, 129.67, 130.15, 137.65, 138.41, 143.71, 147.19, 162.54, 162.90. HRMS (ESI) calc. for $\text{C}_{21}\text{H}_{15}\text{Cl}_2\text{N}_2\text{O}_2$ ($[\text{M} - \text{H}]^-$): 397.05161; found: 397.05133.

3. Crystallisations

PRM3 crystallisations were performed by liquid–liquid or liquid–vapour diffusion using various combinations of solvents with high **PRM3** solubilities (good solvents) and solvents with low **PRM3** solubilities (poor solvents). Good solvents used included CHCl_3 , tetrahydrofuran (THF), toluene, and ethyl acetate (EA), while poor solvents used included cyclohexane, *n*-hexane, diethyl ether, methanol, and ethanol. The growth tubes were maintained at 298 K during both methods, while liquid–vapour diffusion was also performed at 278 K.

4. X-ray structural analysis

The **PRM3** crystal diffraction data were collected at 223 K on a Rigaku XtaLAB PRO diffractometer using graphite-monochromated Mo $K\alpha$ radiation ($\lambda = 0.71073$ Å) for **PRM3V** and Cu $K\alpha$ radiation ($\lambda = 1.54187$ Å) for the other forms. Data reductions were performed using CrysAlis Pro 1.171.39.20a [14]. The crystal structures were determined by direct methods using SHELXT ver. 2018/2 [15] and corrected by the full-matrix least-squares method using SHELXL ver. 2018/3 [16]. All non-H atoms were refined anisotropically, whereas the positions of all H atoms were calculated geometrically using a riding model.

Structural analyses were performed using Olex2-1.2 [17]. The crystal structures were visualised and evaluated using Mercury 4.20 [18].

5. Differential scanning calorimetry (DSC) and powder X-ray diffraction (PXRD)

DSC measurements were conducted in crimped Al pans using a Rigaku Thermo Plus 2 DSC8230 at a heating rate of 10 K/min, with a typical sample weight of 4.0 mg. Powder samples of **PRM3R** and **PRM3O** were characterised before DSC by PXRD, using a Rigaku SmartLab diffractometer with Cu $K\alpha$ radiation ($\lambda = 1.54187 \text{ \AA}$) at room temperature in the 2θ range 5° – 80° .

6. Intermolecular interaction evaluations

The intermolecular interactions within the crystal structures of three of the polymorphs, excluding **PRM3DR**, were evaluated using two calculation methods. Lattice energy calculations were performed using the atom–atom Coulomb-London-Pauli (AA-CLP) model [19]. The H atom positions were normalised using Mercury 4.20 [18] for all calculations. Hirshfeld surface analyses were performed using CrystalExplorer [20]. The calculations used atomic coordinates from each crystal structure.

Results & Discussion

1. PRM3 crystallisation

PRM3 crystallisations were performed with different solvent combinations at 298 K using two methods. For liquid–vapour diffusion, the crystallisations were also performed at 278 K, and the dye solutions were then saturated. The results are summarised in Table 1.

Crystallisation by liquid-liquid diffusion using CHCl_3 as a good solvent results in plate-shaped **PRM3O** when cyclohexane or *n*-hexane is used as the poor solvent. No crystals are obtained from the alcoholic poor solvents. The use of THF results in concomitant crystallisation of plate-shaped **PRM3O** and needle-shaped **PRM3R**, using either cyclohexane or *n*-hexane as poor solvents. Fine, powdered crystals of **PRM3O** are obtained from a combination of toluene and cyclohexane or *n*-hexane and from a combination of EA and cyclohexane or *n*-hexane. For liquid-vapour diffusion, two temperatures were examined for two good solvents, with diethyl ether as the poor solvent. In CHCl_3 , each polymorph was successfully prepared by changing the temperature. Plate-shaped **PRM3O** crystals and needle-shaped **PRM3R** crystals were obtained at 298 and 278 K, respectively. The samples in THF at 278 K yield a differently shaped **PRM3R**, although both polymorphs are concomitantly obtained at 298 K. No **PRM3V** or **PRM3DR** are observed during this examination. The prepared crystals of **PRM3O** and **PRM3R** were stable for at least a few months under ambient conditions.

<Table 1>

2. Thermal responses of PRM3R and PRM3O and the discoveries of further polymorphs

DSC measurements were performed for **PRM3R** and **PRM3O**. Figure 2 shows the DSC thermogram of **PRM3R**, revealing several endothermic peaks. The first sharp peak appears at 343–348 K, while the

second, relatively broad peak is observed at approximately 368–373 K. A small, broad peak is observed at approximately 500–530 K, and finally, a sharp peak is observed at approximately 543 K, which is the melting point of **PRM3**. Meanwhile, the DSC thermogram of **PRM3O** displays a small, broad peak at approximately 500–530 K, with a melting point at approximately 543 K.

We also examined the thermal changes in **PRM3R** and **PRM3O** on a heating plate (Figure 3). The colour of the **PRM3R** crystal changes at approximately 343 K, with a dynamic length extension along the long crystal axis (see movie file 1 in the Supporting Information (SI)). This crystal shows no further transformation upon cooling to room temperature. The obtained crystals maintain crystallinity, and X-ray analysis was successful, indicating that the obtained crystals are vermilion in colour, corresponding to the third polymorph of **PRM3**. This polymorph is denoted as **PRM3V**. Upon further heating, **PRM3V** changes colour at approximately 370 K to orange, with a dynamic behaviour similar to that in the phase transition from **PRM3R** to **PRM3V**. The resultant crystals display no change in appearance upon cooling, with no peak observed in the DSC thermogram upon cooling. Crystallinity is maintained, and the structural analysis shows that the obtained orange crystals are **PRM3O** (Table S1 indicated as **PRM3O'**). When the crystals of **PRM3O** are heated above 500 K, the colour of the sample changes from transparent bright orange to opaque dark red, as shown in Figure 3, corresponding to the small, broad peak at approximately 500–530 K in the DSC thermograms. This reversible phase change between **PRM3O** and the dark red phase was observed several times during heating below 530 K. We obtained dark red crystals for X-ray analysis by heating **PRM3O** crystals at approximately 533 K. Although the analysis still requires further examination, this crystal is characterised as the fourth polymorph of this dye, as shown in the SI (Table S2 and Figure S1).

<Fig. 2>

<Fig. 3>

3. Geometric comparisons of **PRM3R**, **PRM3O**, and **PRM3V**

The crystal structures of **PRM3R**, **PRM3O**, and **PRM3V** were successfully analysed using single-crystal X-ray diffraction. The **PRM3R** and **PRM3O** crystals were obtained by crystallisation, as shown in Table 1, while crystals of **PRM3V** were prepared by heating **PRM3R**. Crystallographic data are listed in Table 2. These three polymorphs belong to the triclinic space group *P*-1.

<Table 2>

3-1. Molecular geometries

The molecular structures of the three polymorphs were examined in detail, particularly focusing on the geometric relationship between the DPP core, phenyl rings, and propyl groups. Their molecular structures are shown in Figure 4, along with a structural overlay. The bond lengths within each polymorph show no significant differences in the dye chromophore with respect to bond alternation. No significant difference is observed in the bond angles in the chromophores within the three polymorphs.

To evaluate the DPP core planarity, we measured the average distance of a set of ten DPP core atoms from their least-squares mean plane. A planar DPP core is observed within all three polymorphs, with the average distance ranging from 0.0121 (**PRM3R**) to 0.0294 Å (**PRM3V**).

<Fig. 4>

The propyl group within each polymorph has an almost planar conformation. Several important dihedral angles are listed in Table 3. The dihedral angle between the planes of the propyl C atoms and the DPP core is almost perpendicular. The propyl C atom bonded to the amino N atom is slightly deviated from the DPP core plane in all polymorphs. The projection direction of the **PRM3V** propyl group is different from those of **PRM3R** and **PRM3O**. The twist angles of the phenyl rings relative to the DPP core are estimated from the dihedral angle between the DPP core plane and the least-squares mean planes of the six phenyl-ring C atoms, with varying results. The phenyl group bonded to the DPP ring on the non-substituted amino side is slightly twisted relative to the DPP core within all three polymorphs, with twist angles of 8.04°, 3.92°, and 0.80° for **PRM3R**, **PRM3V**, and **PRM3O**, respectively. Conversely, the other phenyl ring is twisted relative to the DPP core by approximately 30°, with the **PRM3O** ring twisted in the opposite direction to those of **PRM3R** and **PRM3V**. These structural features are quite different from those observed in our study on three analogous **PR3** polymorphs [11]. In **PR3**, the propyl C atom bonded to each amino N atom were located in the DPP core plane in all polymorphs, with both propyl groups projecting out from the DPP core plane in all three polymorphs. The two phenyl rings were twisted by approximately 40°–50°, although the twist direction varied. We also measured the root-mean-square deviation (RMSD) values of the current three polymorphs using Mercury 4.20, which indicated that there was molecular similarity between **PRM3O** and **PRM3R**. These results and our previous results for **PR3** suggested that the introduction of a flexible propyl group was critical in conformational polymorphism in the chlorinated DPP skeleton, where there is one structure report for chlorinated DPP [21], even though amino substitution reduced or eliminated the formation of strong hydrogen bonds.

3-2. Molecular arrangement and related intermolecular interactions

Within all three polymorphs, DPP dimers were formed by complementary hydrogen bonding. The molecular arrangement of the three polymorphs was characterised by a 2D arrangement of the dimer and stacking of the dye molecules.

Figures 5–7 illustrate the 2D arrangement of the dimer within the three polymorphs. In **PRM3R**, a DPP molecule within the dimer forms two further complementary intermolecular interactions with the adjacent DPP molecule, as shown in Figure 5 (a): a weak hydrogen bond between the phenyl C–H and O=C and a methyl C–H···Cl interaction. Through this interaction, the dimers form a 1D chain-like arrangement. This 1D chain is further linked to the adjacent 1D chain through Cl···Cl interactions, forming an almost planar 2D molecular sheet. As shown in Figure 5 (b), these 2D sheets stack to form the crystal structure. Figure 5 (c) depicts the stacking of three **PRM3R** molecules. One pair is

characterised by the stacked DPP cores, whereas in the other pair, the molecules are stacked with a slippage along the long molecular axis. The former pair is thus a $\pi \cdots \pi$ stacked pair, which is well-known in organic dye crystals. In the latter pair, a complementary halogen $\cdots \pi$ interaction is observed, with the DPP cores less overlapped.

In the molecular arrangement of **PRM3O** and **PRM3V**, the same features as those in **PRM3R** are observed, although the geometries are slightly different, as shown in Figures 6 and 7. Two dimers interact complementarily through a weak hydrogen bond between the phenyl C–H and O=C and the methyl C–H \cdots Cl interaction to form a 1D chain-like arrangement, as observed in **PRM3R**. These 1D chains are linked to adjacent 1D chains, forming a 2D molecular sheet. In **PRM3V**, there is a Cl \cdots Cl short contact between the 1D chains, while there are several contacts involving Cl in **PRM3O**. The DPP cores of the molecules of **PRM3O** are planar to the 2D sheet (Figure 6 b)), whereas the DPP cores of the molecules of **PRM3V** are slightly tilted relative to the 2D sheet (Figure 7 b)). Their molecular stacking arrangements are depicted in Figures 6 c) and 7 c) for **PRM3O** and **PRM3V**, respectively. **PRM3O** stacks in a similar pattern to the molecules in **PRM3R**: one pair is $\pi \cdots \pi$ stacked and the other is slip-stacked. The shift in the latter pair within **PRM3O** is larger relative to that of **PRM3R**. In **PRM3V**, two $\pi \cdots \pi$ stacked pairs are observed.

<Fig. 5>

<Fig. 6>

<Fig. 7>

The arrangements of the dimers within the 2D sheets were compared. The distances between the centres of the dimers (corresponding to the inversion centres) were estimated. The distances along the 1D chain, corresponding to the hydrogen-bonded direction, were similar between the three polymorphs (15.33, 15.43, and 15.84 Å for **PRM3R**, **PRM3O**, and **PRM3V**, respectively). Conversely, the distances between the dimers along the halogen interaction direction of **PRM3R**, **PRM3O**, and **PRM3V** were 18.15, 17.75, and 16.28 Å, respectively. The angles between these two directions were 108.3°, 108.7°, and 104.4° for **PRM3R**, **PRM3O**, and **PRM3V**, respectively. Therefore, there were only slight structural differences in the molecular 2D sheets, suggesting that the differences in the molecular stacking were a key structural factor in the observed thermosalient effect during the phase transitions. This difference in the molecular stacking is also expected to contribute to the colour difference in these polymorphs.

These structural features were further analysed using lattice energy calculations, with the results summarised in Table 4. In all three polymorphs, the pair with the largest contribution to the lattice energy is the $\pi \cdots \pi$ stacked DPP core pair. In **PRM3R** and **PRM3O**, the second largest pair is the hydrogen-bonded dimer pair, and the third largest pair is the weak hydrogen-bonded pair, both of which are involved in the 1D chain formation. In contrast, the second largest pair in **PRM3V** is another $\pi \cdots \pi$ stacked pair, while the third largest pair is a hydrogen-bonded dimer pair. This is consistent with the molecular arrangement characterised by the 1D chain structure of the hydrogen-bonded dimers and their

stacking.

Hirshfeld surface analyses were performed to study the contribution of halogen-related interactions, and the resultant bar chart is presented in Figure 8. The contribution of direct Cl···Cl contacts is 3.6 % in **PRM3R** and 3.0 % in **PRM3O**, while their proportion within **PRM3V** is small (1.0 %). The contribution of the Cl···C interaction is larger (2.9 %) in **PRM3V**, while it is approximately 2 % within **PRM3R** and **PRM3O**. There is no significant difference with respect to the Cl···H interactions. This is consistent with the similar crystal structures of **PRM3R** and **PRM3O**, particularly with respect to the 2D molecular sheet arrangement and stacking, although no Cl···Cl short contacts are observed in **PRM3O**.

<Table 4>

<Fig. 8>

3-3. The fourth polymorph

The DSC thermograms suggest that another phase transition occurs just before the melting point. This transition from **PRM3O** to another phase was visibly observed to be reversible when heating is stopped at approximately 530 K by heating experiment. However, when the **PRM3O** crystal is heated to approximately 533 K, which is just before the melting point, the crystal colour changes from orange to deep red, and the deep red crystal does not change upon cooling to room temperature, as shown in Figure 9. A slight dynamic behaviour is also observed during this phase transition (see movie file 2 in the SI). X-ray structural analysis of these deep red crystals is currently underway, and the preliminary results are shown in the SI (Table S2 and Figure S1). This deep red crystal might be the fourth polymorph (**PRM3DR**) belonging to the triclinic *P*-1 space group. The crystallographic data and molecular structure of **PRM3DR** are almost identical to those of **PRM3V**, but the molecular arrangement of **PRM3DR** differs significantly from that of the other three polymorphs. A more detailed structural comparison will be conducted after obtaining sufficient analytical results for **PRM3DR**.

<Fig. 9>

Conclusion

Four polymorphs of the *N*-propylated DPP dye, **PRM3**, were observed. Two polymorphs, **PRM3R** and **PRM3O**, were prepared by crystallisation using solution methods. The other two polymorphs, **PRM3V** and **PRM3DR**, were obtained by heating **PRM3R** and **PRM3O**, respectively. Additionally, **PRM3V** converted to **PRM3O** upon heating. Therefore, this tetramorphic system was characterised by a three-step thermal phase transition. During each transition, crystallinity was maintained with a thermosalient effect. In particular, crystal deformation was observed. Detailed crystal structure analyses revealed that structural differences in the stacking may contribute to the thermosalient effect.

CRedit authorship contribution statement

Yusuke Kikuchi: Investigation, Methodology, Visualization, Writing - Original Draft

Shinya Matsumoto: Conceptualization and Supervision, Visualization, Writing - Review & Editing

Conflicts of interest

There are no conflicts of interest to declare.

Acknowledgements

The authors thank Mr. Shinji Ishihara of Yokohama National University for his kind support in the NMR, IR, and mass spectra measurements. The authors also thank Mr Tenma Muroya and Dr. Sung-Hoon Kim of Yokohama National University for preparation of the movie files. English language editing was done by Editage (www.editage.com).

References

- [1] a) P. Naumov, *Chem. Rev.*, 2015, **115**, 12440–12490, b) P. Naumov, *J. Am. Chem. Soc.*, 2010, **132**, 11566–11579, c) S. Saha, *Acc. Chem. Res.*, 2018, **51**, 2957–2967.
- [2] P. Fratzl and F. G. Barth, *Nature*, 2009, **462**, 442–448.
- [3] S. Lv, D. M. Dudek, Y. Cao, M. M. Balamurali, J. Gosline, and H. N. Li, *Nature*, 2010, **465**, 69–73.
- [4] M. Morimoto and M. Irie, *J. Am. Chem. Soc.*, 2010, **132**, 14172–14178.
- [5] M. C. Etter and A. R. Siedle, *J. Am. Chem. Soc.*, 1983, **105**, 641–643.
- [6] K. Hunger and M. U. Schmidt, *Industrial Organic Pigments, fourth completely revised edition.*, Wiley-VCH, 2018.
- [7] P. Data, *J. Phys. Chem. C*, 2016, **120**, 2070–2078.
- [8] Y. W. Soon, *Chem. Commun.*, 2013, **49**, 1291–1293.
- [9] S. S. Mali and C. K. Hong, *Nanoscale*, 2016, **8**, 10528–10540.
- [10] H.-S. So, T. Minami, T. Jindo, and S. Matsumoto, *CrystEngComm*, 2018, **20**, 5317–5320.
- [11] H.-S. So and S. Matsumoto, *Acta Cryst.*, 2019, **B75**, 414–422.
- [12] R. G. Simões, C. E. S. Bernardes, A. Joseph, M. Fátima, M. Piedade, W. Kraus, F. Emmerling, H. P. Diogo, and M. E. M. da Piedade, *Mol. Pharmaceutics*, 2018, **15**, 5349–5360.
- [13] S.-H. Choi, O.-T. Kwon, N.-R. Kim, C. Yoon, J.-P. Kim, and J.-H. Choi, *Bull. Korean Chem. Soc.*, 2010, **31**, 1073–1076.
- [14] CrysAlisPro: Data Collection and Processing Software, Rigaku Corporation (2015). Tokyo 196-8666, Japan.
- [15] G. M. Sheldrick, *Acta Cryst.*, 2014, **A70**, C1437.
- [16] G. M. Sheldrick, *Acta Cryst.*, 2015, **C71**, 3–8.
- [17] Olex2: O. V. Dolomanov, L. J. Bourhis, R. J. Gildea, J. A. K. Howard, and H. Puschmann, *J. Appl. Cryst.*, 2009, **42**, 229–341.
- [18] Mercury 4.20: C. F. Macrae, P. R. Edgington, P. McCabe, E. Pidcock, G. P. Shields, R. Taylor, M. Towler, and J. van de Streek, *J. Appl. Cryst.*, 2006, **39**, 453–457.
- [19] A. Gavezzotti, *New J. Chem.*, 2011, **35**, 1360–1368.
- [20] J. J. McKinnon, M. A. Spackman, and A. S. Mitchell, *Acta Cryst.*, 2004, **B60**, 627–668.
- [21] J. Mizuguchi, A. Grubenmann, and G. Rihs, *Acta Cryst.*, 1993, **B49**, 1056–1060.

Figure legends

Figure 1 Molecular structure of **PRM3**.

Figure 2 Differential scanning calorimetry thermogram of **PRM3R**.

Figure 3 Thermal changes in a **PRM3** crystal.

Figure 4 Molecular structures of a) **PRM3R**, b) **PRM3O**, and c) **PRM3V**, shown in the ORTEP style at the 50 % probability level. d) Their structural overlay in the wireframe style.

Figure 5 Molecular arrangement of **PRM3R**: a) a 2D sheet on the (122) plane based on the hydrogen-bonded dimer viewed from the direction perpendicular to the (122) plane, with hydrogen bonds, including C-H \cdots Cl interactions and Cl \cdots Cl interactions depicted as black and orange dotted lines, respectively, b) two 2D sheets viewed from the direction in the plane of the sheets, c) molecular stacking of three molecules. The molecular pairs contributing significantly to the lattice energy are labelled as [1], [2], and [3] for the 1st, 2nd, and 3rd pairs listed in Table 4, respectively.

Figure 6 Molecular arrangement of **PRM3O**: a) a 2D sheet on the (1-12) plane based on the hydrogen-bonded dimer viewed from the direction perpendicular to the (1-12) plane, with hydrogen bonds depicted as black dotted lines, b) two 2D sheets viewed from the direction in the plane of the sheets, c) molecular stacking of three molecules. The molecular pairs contributing significantly to the lattice energy are labelled as [1], [2], and [3] for the 1st, 2nd, and 3rd pairs listed in Table 4, respectively.

Figure 7 Molecular arrangement of **PRM3V**: a) a 2D sheet almost on the (2-1-2) plane based on the hydrogen-bonded dimer viewed from the direction perpendicular to the sheet, with hydrogen bonds, including C-H \cdots Cl interactions, and Cl \cdots Cl interactions depicted as black and orange dotted lines, respectively, b) Two 2D sheets viewed from the direction in the plane of the sheets, c) molecular stacking of three molecules. The molecular pairs contributing significantly to the lattice energy are labelled as [1], [2], and [3] for the 1st, 2nd, and 3rd pairs listed in Table 4, respectively.

Figure 8 Relative contributions of the halogen interactions to the Hirshfeld surface areas of the three polymorphs.

Figure 9 The phase transition from **PRM3O** to the fourth polymorph (**PRM3DR**).

Table legends

Table 1 **PRM3** crystallisations.

Table 2 Crystallographic data of **PRM3R**, **PRM3O**, and **PRM3V**.

Table 3 Dihedral angles between the DPP core and three groups.

Table 4 Total lattice energies of all molecular pairs and the contributions of the three major molecular pairs.

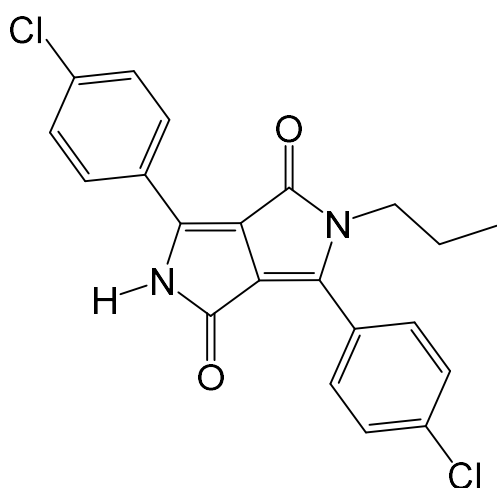


Figure 1 Molecular structure of **PRM3**.

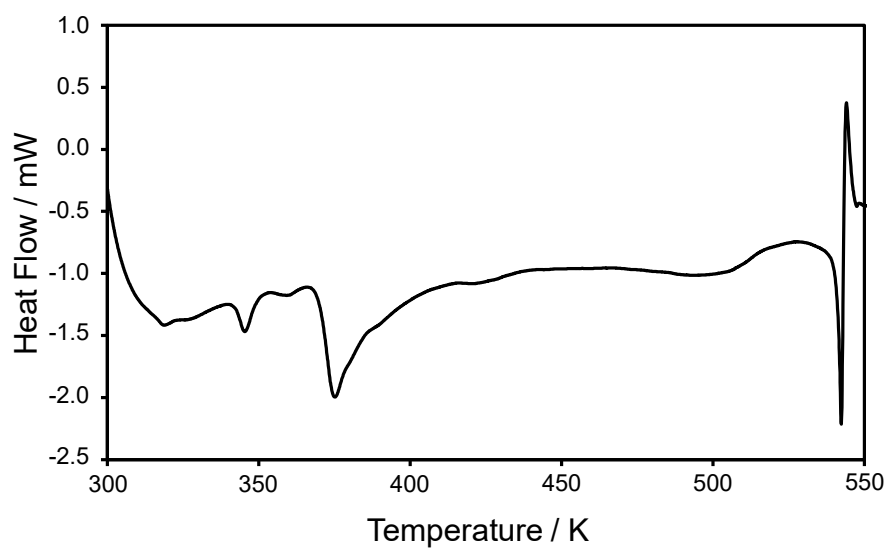


Figure 2 Differential scanning calorimetry thermogram of **PRM3R**.

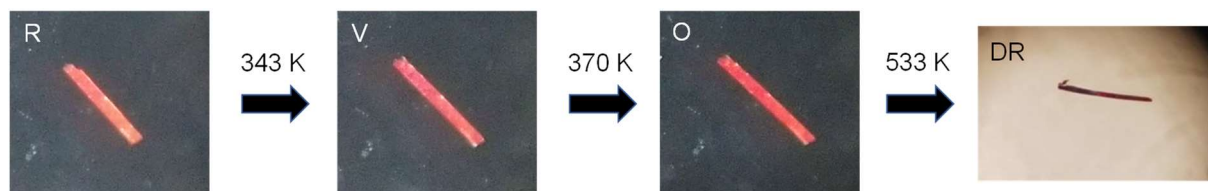


Figure 3 Thermal changes in a **PRM3** crystal.

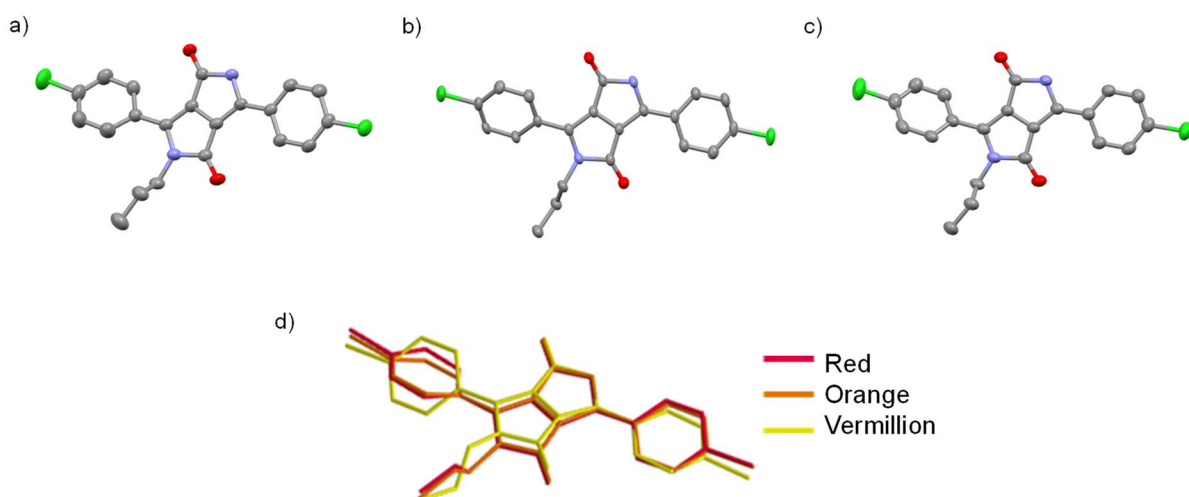


Figure 4 Molecular structures of a) **PRM3R**, b) **PRM3O**, and c) **PRM3V**, shown in the ORTEP style at the 50 % probability level. d) Their structural overlay in the wireframe style.

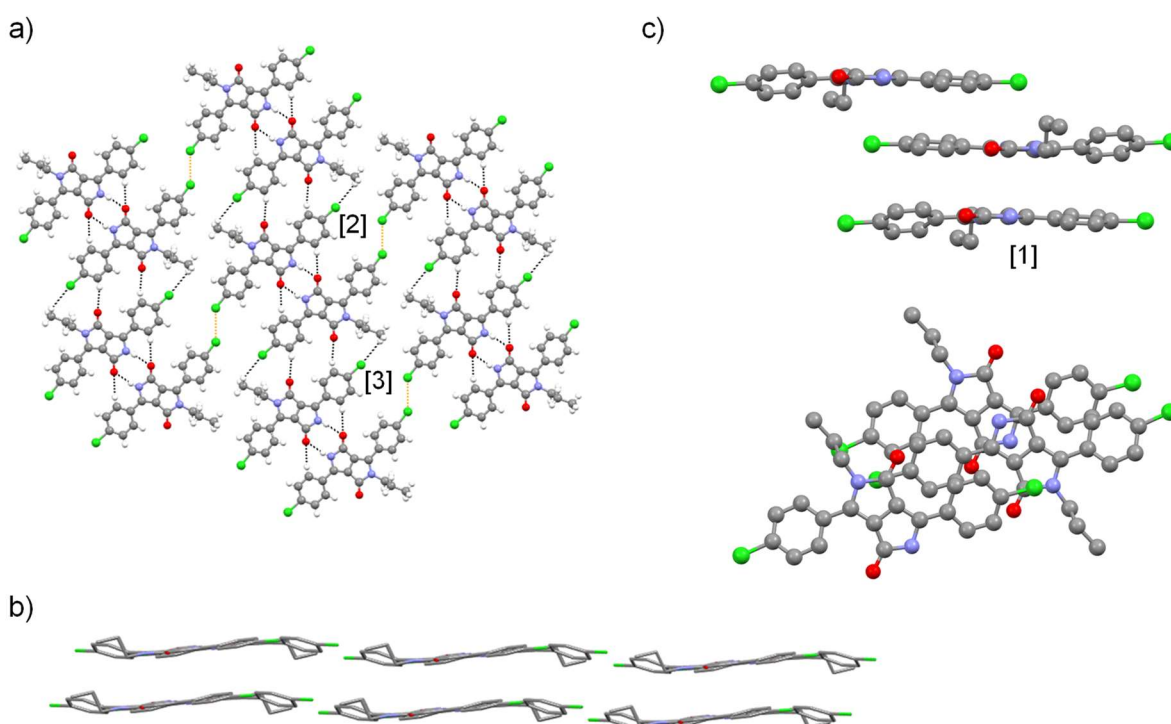


Figure 5 Molecular arrangement of **PRM3R**: a) a 2D sheet on the (122) plane based on the hydrogen-bonded dimer viewed from the direction perpendicular to the (122) plane, with hydrogen bonds, including C-H...Cl interactions and Cl...Cl interactions depicted as black and orange dotted lines, respectively, b) two 2D sheets viewed from the direction in the plane of the sheets, c) molecular stacking of three molecules. The molecular pairs contributing significantly to the lattice energy are labelled as [1], [2], and [3] for the 1st, 2nd, and 3rd pairs listed in Table 4, respectively.

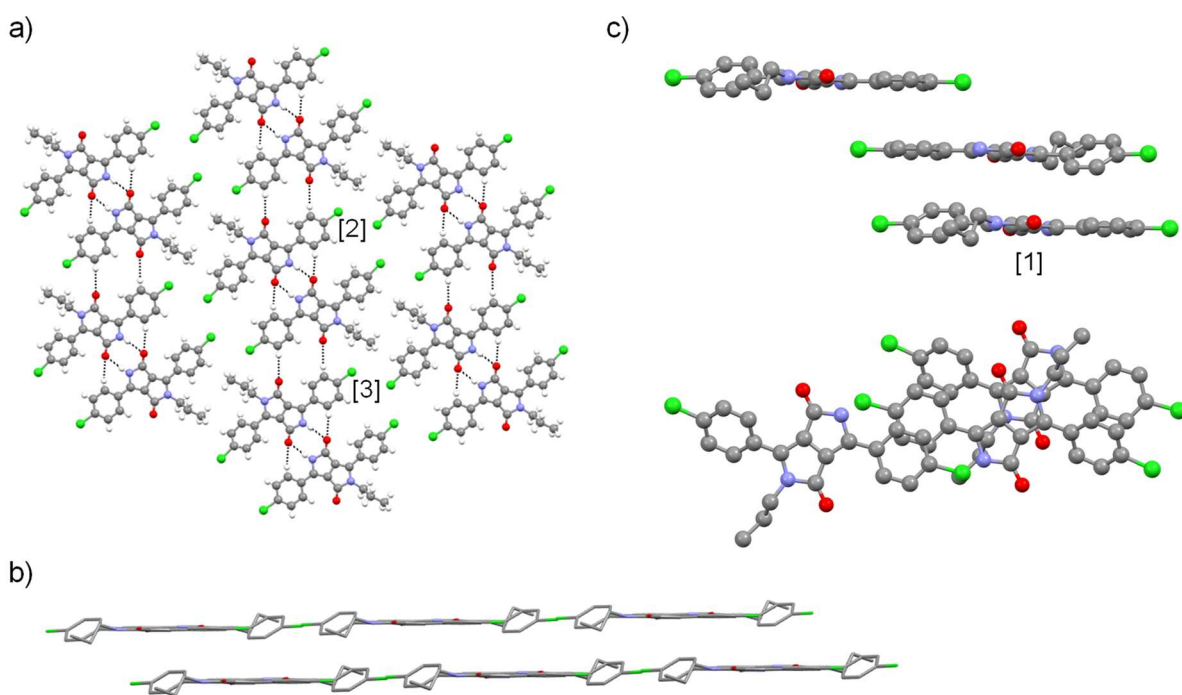


Figure 6 Molecular arrangement of **PRM3O**: a) a 2D sheet on the (1-12) plane based on the hydrogen-bonded dimer viewed from the direction perpendicular to the (1-12) plane, with hydrogen bonds depicted as black dotted lines, b) two 2D sheets viewed from the direction in the plane of the sheets, c) molecular stacking of three molecules. The molecular pairs contributing significantly to the lattice energy are labelled as [1], [2], and [3] for the 1st, 2nd, and 3rd pairs listed in Table 4, respectively.

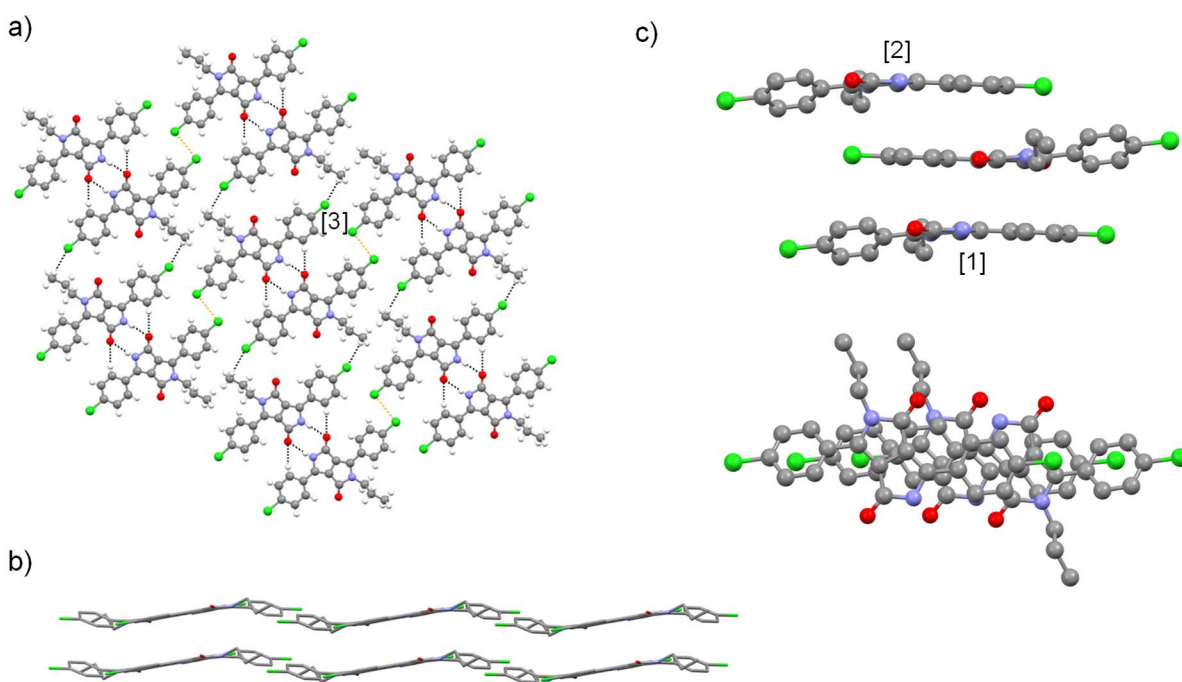


Figure 7 Molecular arrangement of **PRM3V**: a) a 2D sheet almost on the (2-1-2) plane based on the hydrogen-bonded dimer viewed from the direction perpendicular to the sheet, with hydrogen bonds, including C-H \cdots Cl interactions, and Cl \cdots Cl interactions depicted as black and orange dotted lines, b) two 2D sheets viewed from the direction in the plane of the sheets, c) molecular stacking of three molecules. The molecular pairs contributing significantly to the lattice energy are labelled as [1] and [2] for the 1st and 2nd pairs listed in Table 4, respectively.

respectively, b) Two 2D sheets viewed from the direction in the plane of the sheets, c) molecular stacking of three molecules. The molecular pairs contributing significantly to the lattice energy are labelled as [1], [2], and [3] for the 1st, 2nd, and 3rd pairs listed in Table 4, respectively.

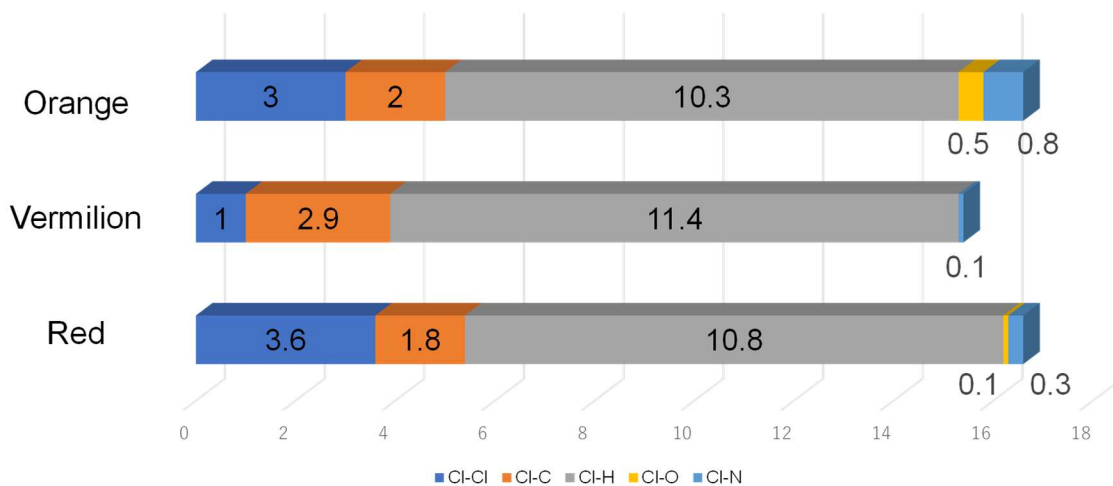


Figure 8 Relative contributions of the halogen interactions to the Hirshfeld surface areas of the three polymorphs.

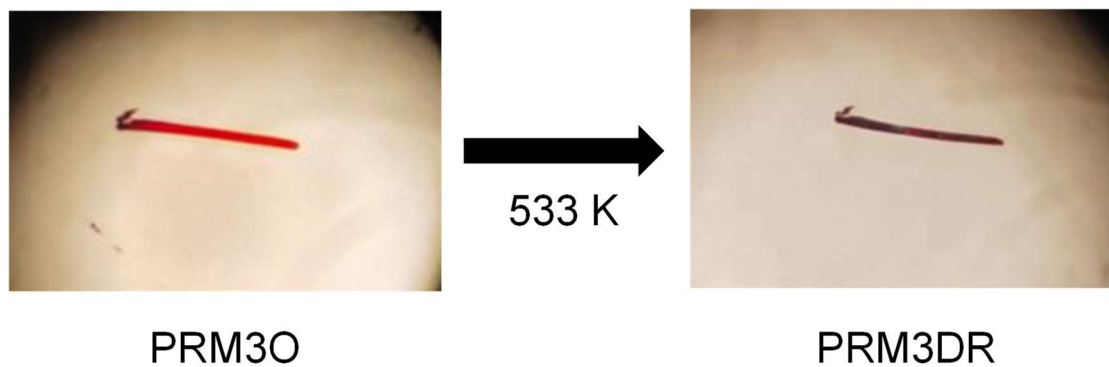


Figure 9 The phase transition from **PRM3O** to the fourth polymorph (**PRM3DR**).

Table 1 **PRM3** crystallisations.

Method	Good solvent	Poor solvent	Temperature / K	Attempts	Crystal colour	Crystal shape
liquid-liquid	CHCl ₃	n-hex	298	4	Orange	Plate
		c-hex	298	4	Orange	Plate
		MeOH	298	2	-	-
		EtOH	298	2	-	-
	THF	n-hex	298	4	Orange, Red	Plate (Orange), Needle (Red)
		c-hex	298	4	Orange, Red	Plate (Orange), Needle (Red)
		MeOH	298	2	-	-
		EtOH	298	2	-	-
	toluene	n-hex	298	2	Orange	Powder
		c-hex	298	2	Orange	
		MeOH	298	2	-	-
		EtOH	298	2	-	-
	EA	n-hex	298	2	Orange	Powder
		c-hex	298	2	Orange	
		MeOH	298	2	-	-
		EtOH	298	2	-	-
liquid-vapour	CHCl ₃	ether	298	20	Orange	Plate
			278	4	Red	Needle
	THF		298	4	Orange, Red	Plate (Orange), Needle (Red)
			278	20	Red	Plate and Needle

THF = tetrahydrofuran, EA = ethyl acetate, n-hex = *n*-hexane, c-hex = cyclohexane, MeOH = methanol, EtOH = ethanol.

Table 2 Crystallographic data of **PRM3R**, **PRM3O**, and **PRM3V**.

	PRM3R	PRM3O	PRM3V
Formula	C ₂₁ H ₁₆ N ₂ O ₂ Cl ₂	C ₂₁ H ₁₆ N ₂ O ₂ Cl ₂	C ₂₁ H ₁₆ N ₂ O ₂ Cl ₂
Crystal size / mm	0.283 x 0.066 x 0.025	0.311 x 0.166 x 0.047	0.756 x 0.100 x 0.029
Crystal system	Triclinic	Triclinic	Triclinic
Molecular weight	399.27	399.27	399.27
Space group	<i>P</i> -1	<i>P</i> -1	<i>P</i> -1
<i>a</i> / Å	6.1089(2)	10.0941(2)	7.5775(9)
<i>b</i> / Å	9.6567(5)	10.1582(2)	7.9456(8)
<i>c</i> / Å	15.8773(6)	10.8283(3)	16.2096(13)
α / °	87.008(4)	63.183(2)	103.927(8)
β / °	88.263(3)	70.379(2)	96.226(8)
γ / °	88.159(3)	80.704(2)	104.186(10)
<i>V</i> / Å ³	934.49(7)	933.30(4)	903.71(17)
<i>Z</i>	2	2	2
Reflections collected	8759	9702	14758
Independent reflections	3600	3618	4700
Temperature / K	223	223	223
<i>D</i> _{calc} / g cm ⁻³	1.419	1.421	1.460
<i>R</i> _{int}	0.0476	0.0327	0.0625
<i>R</i>	0.0555	0.0426	0.0547
<i>wR</i> ₂ (all data)	0.1754	0.1480	0.1571
CCDC No.	2073287	2073288	2073289

Table 3 Dihedral angles between the DPP core and three groups.

	Dihedral angle* / °		
	DPP and Ph1	DPP and Ph2	DPP and Pr
PRM3R	8.04	25.08	173.09
PRM3O	0.80	-35.66	176.22
PRM3V	3.92	30.84	173.25

* Dihedral angles between the DPP core and several groups. Ph1 is the phenyl ring bonded to the DPP ring on the non-substituted amino side and Ph2 is the phenyl ring on the opposite side. DPP and Pr is the angle between the DPP core and the plane of the propyl C-atoms.

Table 4 Total lattice energies of all molecular pairs and the contributions of the three major molecular pairs.

	Total energy* (kJ/mol)	The most stable pair (kJ/mol)	The second stable pair (kJ/mol)	The third stable pair (kJ/mol)
PRM3R	-182.3	-65.1 (20.1 %)	-59.8 (18.5 %)	-34.7 (10.7 %)
PRM3O	-177.2	-72.8 (22.7 %)	-58.0 (18.1 %)	-28.8 (9.0 %)
PRM3V	-190.3	-83.6 (24.1 %)	-72.7 (21.0 %)	-33.9 (9.8 %)

* The total energy of all molecular pairs is the summation of the energies of all calculated molecular pairs. Half of the total energy corresponds to the lattice energy.